New calculation method of neutron kerma coefficients for carbon and oxygen below 30 MeV

Xiaojun Sun* and Wenjing Qu
College of Physics and Electronic Engineering, Guangxi Normal University, Guilin 541004, People's Republic of China

Junfeng Duan and Jingshang Zhang
China Institute of Atomic Energy, P. O. Box 275(41), Beijing 102413, People's Republic of China

(Received 7 May 2008; published 26 November 2008; publisher error corrected 28 July 2009)

On the basis of the statistical theory of a neutron-induced light nucleus reaction, a new kerma coefficient calculation formula, expressed as $k_\Phi = N\sum_{ijk}\overline{E}_{ijk}(E_n)\sigma_{ijk}(E_n)$, is developed in this paper. In an analysis of the $n + {}^{12}$C and $n + {}^{16}$O reactions below 30 MeV, the average energies $\overline{E}_{ijk}$ of emitted particles of all kinds in the laboratory frame are derived in detail for different channels, allowing an exact energy balance. The optical model parameters of neutron and charged particles, which had reproduced very well the outgoing neutron double-differential cross sections in our early works, are used to obtain the cross sections σ_{ijk}. The calculated partial, elastic recoil, and total kerma coefficients for carbon and oxygen are consistent with existing experimental kerma coefficient data. The elastic cross sections and the first Legendre coefficients of elastic angular distribution derived from EBDF/B-VIIb3 are used in this paper to improve significantly the elastic recoil and total kerma coefficients.

DOI: 10.1103/PhysRevC.78.054610 PACS number(s): 24.10.−i, 25.40.−h, 28.20.−v, 87.53.Bn

I. INTRODUCTION

Some biologically important elements, such as carbon and oxygen, are the main constituents of tissues and tissue substitutes. Reactions of fast neutrons with carbon and oxygen that lead to charged-particle emission have great importance in neutron dosimetry, biological effectiveness of neutron irradiations, and neutron heating of carbon- or oxygen-containing materials in fission and conceptual fusion reactors. The key response function for heating is the kerma coefficient. Here, kerma K (an acronym for kinetic energy released in matter) describes the transfer of energy from indirectly ionizing radiation into kinetic energy of charged particles, and the kerma coefficient represents the subsequent interaction of these charged particles with matter depositing energy by ionization and excitation, i.e., the energy deposited per unit mass [1]. The neutron kerma coefficients of carbon and oxygen are needed in the determination of radiation shielding requirements for radiation protection purposes, optimization of dose delivery to a treatment volume, decisions on biological effectiveness of different therapy beams, etc.

Two independent methods are used to derive experimental neutron kerma coefficients. The first method is based on dosimetric methods to determine kerma K, which is closely related to absorbed dose D, and the measurement of Φ (the number of neutrons per unit area). The ratio of the two quantities gives the total kerma coefficient k_Φ according to its definition $k_\Phi = K/\Phi \approx D/\Phi$ [1]. This direct measurement of kerma coefficients is difficult, and the measured values are available only for a few elements and neutron energies. Moreover, such measurements require total particle equilibrium in the studied volume and necessitate significant corrections [2]. The second method uses experimental cross sections, which requires information on all significant reaction channels, including angular and/or energy distribution and energy-angle distribution of secondary particle. For a given energy of incident neutron E_n and target nuclide, the kerma coefficient is given by [3]

$$k_\Phi(E_n) = N\sum_i \int E \int \frac{d^2\sigma_i(E_n)}{d\Omega\, dE}\, d\Omega\, dE. \qquad (1)$$

The coefficient $N = 9.64853/M_A$, where M_A is the atomic mass of the target in units of u, converts the kerma coefficient from units of MeV b to S.I. units of fGy m^2. E is the energy of ejectile i, and $d^2\sigma_i(E_n)/d\Omega/dE$ is the double-differential cross section of ejectile i at incident neutron energy E_n. Unfortunately, below 30 MeV, the double-differential cross sections of the ejectile, even including the neutron, are sparse for carbon and oxygen. So the experimental kerma coefficients for these important nuclides are obtained from the experimental energy-differential cross sections according to the formula [4,5]

$$k_\Phi = N\sum_i \left(\frac{d\sigma}{dE}\right)_i E_i\, \Delta E_i, \qquad (2)$$

where E_i is the centroid of the energy bins of width ΔE_i, and $(d\sigma/dE)_i$ is the energy-differential cross section for ejectile i.

Evaluation kerma coefficients below 20 MeV were derived from ENDF/B-VI format libraries using such data processing codes as NJOY [6], MAZE [7], and MCNP [8]. These codes take advantage of the fact that many evaluations give explicit energy distributions for the emitted neutrons and photons. The energies needed for the kerma coefficient can be obtained by subtracting the average emitted energies of the neutrons and photons from the available energy. The limitation using data processing codes on the accuracy of the neutron kerma calculation is determined by the availability and accuracy of the evaluation libraries. The information on all

*sxj0212@mailbox.gxnu.edu.cn

charged-particle emission cross sections in the well-known libraries, such as ENDF/B-VIIb3, JENDL-3.3, etc., and their earlier versions, is incomplete. For example, the outgoing neutron double-differential cross sections, which are related to the charged-particle emission, were not given in ENDF/B-VIIb3 and JENDL-3.3 for carbon below 20 MeV. The energy-angle spectra of oxygen from ENDF/B-VIIb3 were only determined by an isotropic method. This problem originates from two sources. First, the evaluations were generally produced for applications in neutron transport, and energy deposition was not a primary concern, leading sometimes to several charged-particle cross sections being lumped into a single cross section. This would faintly affect neutron transport but could give significantly incorrect values of the kerma coefficient. Second, the emission mechanism for neutron-induced light nuclear reactions, in which all the emitted particles proceed between discrete levels, is very complex, and the strong recoil effect must be strictly taken into account.

For neutron energies above 20 MeV, kerma coefficients are obtained directly from the cross sections in the laboratory frame calculated by a theory model code such as GNASH [9]. Partial kerma coefficients for each type of secondary charged particle are determined using [9]

$$k_{\Phi}^{i} = N\overline{\varepsilon}_i \sigma_i^{\text{prod}}, \tag{3}$$

where k_{Φ}^{i} is the partial kerma coefficient of ejectile type i, σ_i^{prod} is the inclusive production cross section of ejectile i expressed in barns, and $\overline{\varepsilon}_i$ is the average energy of ejectile i expressed in MeV. The terms in formula (3) have incomplete information on the parameters below 30 MeV, for example, the different channel, the levels of the residual nuclide, and so on. In analyzing the reaction mechanism, one can see that there are many accessible reaction channels for carbon and oxygen in this energy region, as listed in Sec. III.

Based on the unified Hauser-Feshbach and exciton model, a statistical theory of neutron-induced light nucleus reaction was proposed in 1999 [10]. The key point of this statistical theory is that it properly takes into account the conservation of energy, angular momentum, and parity in the emissions from the discrete levels of the compound nucleus to the discrete levels of the residual nuclei with the preequilibrium mechanism, which dominates the reaction processes in neutron-induced light nucleus reactions. Obviously, if the parity and angular momentum effects are not considered, the theory would be reduced to the exciton model [11]; whereas if the preequilibrium effect is omitted, it is reduced to the Hauser-Feshbach model [12]. With the more accurate detection of the level schemes of light nuclei [13,14] and the intensive studies of the various emission mechanisms for neutron-induced different light nucleus reactions, the theoretical results of the neutron double-differential cross sections for different targets were gradually improved over the past decade, for example, for ^{6}Li [15], ^{7}Li [16], ^{10}B [17], ^{11}B [18], ^{12}C [19], ^{14}N [20], ^{16}O [21], and ^{19}F [22]. The detailed description of this statistical theory is given in Ref. [23]. For neutron interactions with tissue, water, and tissue substitutes, carbon and oxygen are the most important elements besides hydrogen. In this paper, a new calculation method is developed to obtain the neutron kerma coefficients of carbon and oxygen on the basis of this statistical theory. These calculated values, including all type of charged-particle partial kerma coefficients, elastic recoil and total kerma coefficients, agree well with the existing measurements.

This paper proceeds as follows. In Sec. II, the formula used to determine the total and/or partial kerma coefficients is described. In Sec. III, we list all accessible channels below 30 MeV and energy expressions carried by emitted particles for $n + {}^{12}$C and $n + {}^{16}$O reactions. Our calculated results for carbon and oxygen are given in Sec. IV and further discussions are presented in the last section. The statistical theory of neutron-induced light nucleus reactions is also introduced succinctly in Appendix A, and the relative formulas are derived in detail for different particle emissions in Appendix B.

II. FORMULA FOR KERMA COEFFICIENTS

The total kerma coefficient for a given neutron incident energy E_n is partitioned into the partial contributions from the light ($A \leqslant 6$) charged particles, the nonelastic recoils ($A > 6$), and the elastic recoils. For a given target nuclide, the total kerma coefficient is given by

$$k_{\Phi} = \sum_{i} k_{\Phi}^{i} = N \sum_{ijk} \overline{E}_{ijk}(E_n)\sigma_{ijk}(E_n), \tag{4}$$

where $\overline{E}_{ijk}$ and σ_{ijk} are the average energy (expressed in MeV) and the production cross section (in barns) in the laboratory frame, respectively. Here, i denotes the type of charged particle including light charged particles and recoils, j denotes the type of reaction channels, and k indicates the excitation energy level of the residual nucleus which can emit the secondary and/or third particle, or proceed via two-body separation, or carry out γ decay. The coefficient N is identical with the value of formulas (1)–(3). Obviously, the terms in formula (4) contain more comprehensive parameter information than those in formula (3).

For nonelastic processes of neutron-induced light nucleus reaction, the LUNF code [10] was used to calculate the cross sections of different channels (including elastic and inelastic channels), angular distributions, and the double-differential cross sections. This code treats neutron-induced light nucleus reactions as proceeding through an initial preequilibrium emission mechanism between discrete levels, followed by a process of sequential particle emission from decaying compound nuclei, until the final residual nucleus attains its ground state via γ-ray emission. The dynamics of this statistical theory is introduced succinctly in Appendix A.

The phenomenological spherical optical potential is employed in the model calculation. Two new sets of neutron optical potential parameters for carbon and oxygen are adjusted by the APMN code [24], which takes the level schemes of target and residual nuclei as the input parameters and can automatically search the optimal optical potential parameters to fairly fit the variously measured cross sections, such as the total cross section, elastic and inelastic scattering cross section, elastic scattering angular distributions, and nonelastic

scattering cross section. This adjustment procedure is different from the calculation of cross sections in Ref. [9] for light elements. The total outgoing neutron double-differential cross sections calculated by the LUNF code agree fairly well with the measurements in our earlier works for carbon and oxygen elements [19,21]. Therefore, the optical potential parameters of the charged particles ($A < 6$) for $n + {}^{12}$C and $n + {}^{16}$O in this paper are obtained by the LUNF code. It should be mentioned that the optical model calculation cannot reproduce the specific structures of elastic, inelastic, and total cross sections in the low incident energy region, but it can show reasonably their tendencies, especially in higher energy region, as mentioned in Sec. VIII of Ref. [10].

III. REACTION CHANNEL ANALYSIS AND ENERGY EXPRESSIONS

A. For the $n + {}^{12}$C reaction

The binding energy B can be expressed as

$$B_i = \Delta m_i + \Delta M_i - \Delta M_{i-1}, \tag{5}$$

where Δm_i and ΔM_i are the mass excesses of the ith emitted particle and its residual nucleus (ΔM_0 is the mass excess of compound nucleus), respectively. The reaction energy is given as

$$Q = \Delta m_n + \Delta m_T - \sum_{i}^{i_{\max}} \Delta m_i - \Delta M_{i_{\max}}, \tag{6}$$

where Δm_n and ΔM_T are the mass excesses of the neutron and target nucleus, respectively, and $\Delta M_{i_{\max}}$ is the mass excess of the last residual nucleus. In this paper, the mass excesses of all kinds of particles and nuclides are derived from Ref. [25]. Therefore, the threshold energy of the different channels is given as

$$E_{\text{th}} = \max\left\{0, -\frac{M_C}{M_T}Q\right\}, \tag{7}$$

where M_C is the mass of the compound nucleus, and M_T is the mass of the target nucleus. Here, function $\max\{x_1, x_2\} = x_1$ if $x_1 > x_2$; otherwise, $\max\{x_1, x_2\} = x_2$.

In terms of formulas (5)–(7), the information for the $n + {}^{12}$C reaction channels is listed in detail in Table I, at incident neutron energy E_n up to 30 MeV. After considering the effect of the Coulomb barrier, the channels at $25 < E_{\text{th}} < 30$ MeV are omitted, because their cross sections are too small to be measured.

Based on the unified Hauser-Feshbach and exciton model, the statistical theory of the neutron-induced light nucleus reaction was developed by Zhang JingShang *et al.* (see Appendix A). The average energies carried by each type of outgoing particle from various residual nucleus levels in different reaction channels can be obtained in analytical expressions (see Appendix B), and the energy balance is held exactly. For convenience, we reexpress some formulas [Eqs. (9)–(18) as follows] derived from Ref. [10].

TABLE I. Accessible reaction channels, binding energy B, Q value, and threshold energy E_{th} for the $n + {}^{12}$C reaction at $E_n \leqslant 30$ MeV. The unit of B, Q, and E_{th} is MeV. Note: the (n, n') channel includes the elastic scattering channel ($E_{\text{th}} = 0.0$).

No.	Channel	B	Q	E_{th}
1	(n, γ)	0.000	4.946	0.000
2	(n, n')	4.946	0.000	4.439
3	(n, p)	17.533	−12.587	13.645
4	(n, α)	10.646	−5.700	6.179
5	(n, d)	18.679	−13.733	14.887
6	(n, t)	23.875	−18.929	20.520
7	$(n,{}^3\text{He})$	24.413	−19.467	21.103
8	$(n,{}^5\text{He})$	13.206	−8.260	8.954
9	$(n,{}^6\text{Li})$	25.867	−20.921	22.680
10	$(n, 2n)$	18.721	−18.721	20.295
11	(n, np)	15.957	−15.957	17.298
12	$(n, n\alpha)$	7.365	−7.365	7.984
13	(n, pn)	3.370	−15.957	17.298
14	$(n, p\alpha)$	10.000	−22.587	24.486
15	$(n, \alpha n)$	1.665	−7.365	7.984
16	$(n, \alpha p)$	16.887	−22.587	24.486
17	$(n, 2\alpha)$	2.467	−8.167	8.854
18	$(n, \alpha d)$	16.696	−22.396	24.279
19	$(n, d\alpha)$	8.663	−22.396	24.279

For the (n, γ) channel, the average recoil kinetic energy $\overline{E}_{M_C}$ of the compound nucleus in the laboratory frame released by γ decay is expressed as

$$\overline{E}_{M_C} = E_n + B_n - E_k, \tag{8}$$

where M_C and m_n are the masses of the compound nucleus and incident neutron, respectively, and E_k is the kth discrete level energy of compound. In terms of formula (4), the partial kerma coefficients of the (n, γ) reaction channel can be easily calculated. However, the cross section of the (n, γ) is too small (<0.3 mb below 30 MeV incident neutron energy) to consider its contribution.

For (n, n), (n, n'), (n, p), (n, α), (n, d), (n, t), $(n,{}^3\text{He})$, and $(n,{}^6\text{Li})$ reaction channels listed in Table I, the average energies carried by the first emitted particle and its residual nucleus in the laboratory frame are given by

$$\overline{E}_{m_1} = \frac{m_n m_1}{M_C^2}E_n + E_{c,K_1}^{m_1} + 2\frac{\sqrt{m_n m_1 E_n E_{c,K_1}^{m_1}}}{M_C} f_1^{m_1}, \tag{9}$$

and

$$\overline{E}_{M_1} = \frac{m_n M_1}{M_C^2}E_n + E_{c,K_1}^{M_1} + 2\frac{\sqrt{m_n M_1 E_n E_{c,K_1}^{M_1}}}{M_C} f_1^{M_1}. \tag{10}$$

Where, m_1 and M_1 are masses of the first emitted particle and its residual nucleus, respectively. $E_{c,k_1}^{m_1}$ and $E_{c,k_1}^{M_1}$, expressed as

$$\begin{aligned} E_{c,k_1}^{m_1} &= \frac{M_1}{M_C}\left(E^* - B_1 - E_{k_1}\right), \\ E_{c,k_1}^{M_1} &= \frac{m_1}{M_C}\left(E^* - B_1 - E_{k_1}\right), \end{aligned} \tag{11}$$

are the energies carried by the first emitted particle m_1 and its residual nucleus M_1 in the center-of-mass frame, where E^* is the excitation energy of compound nucleus, E_{k_1} is the k_1th level energy of M_1, and B_1 is the binding energy of the m_1 particle in the compound nucleus (see Appendix B1). Here, the angular distributions of a single outgoing particle and its residual nucleus are presented as a Legendre polynomial series in the center-of-mass frame, i.e.,

$$\frac{d\sigma}{d\Omega_c^{m_1(M_1)}} = \sum_l \frac{2l+1}{4\pi} f_l^{m_1(M_1)} P_l\left(\cos\theta_c^{m_1(M_1)}\right). \quad (12)$$

This expression is recommended by IAEA Nuclear Data Services as standard ENDF-6 formats, as shown in Sec. IV of Ref. [26]. The first-order Legendre expansion coefficients $f_1^{m_1}$ and $f_1^{M_1}(=-f_1^{m_1})$ of the first emitted particle and its corresponding residual nucleus can be obtained by the linear momentum dependent exciton state density model for an outgoing single nucleon [27] and by the pickup method for composite particle emissions [28].

When the secondary particle m_2 is emitted from M_1 of energy level E_{k_1}, such as the channels from the 10th to the 19th listed in Table I, the average energy carried by the first emitted particle is obtained by Eq. (9). The average energies carried by m_2 and its residual nucleus M_2 are obtained by

$$\overline{E}_{m_2} = \frac{m_n m_2}{M_C^2} E_n + E_{c,k_2}^{m_2} - \frac{2m_2}{M_1 M_C}\sqrt{m_n m_1 E_n E_{c,k_1}^{m_1}}\, f_1^{m_1}, \quad (13)$$

and

$$\overline{E}_{M_2} = \frac{m_n M_2}{M_C^2} E_n + E_{c,k_2}^{M_2} - \frac{2M_2}{M_1 M_C}\sqrt{m_n m_1 E_n E_{c,k_1}^{m_1}}\, f_1^{m_1}. \quad (14)$$

Here, $E_{c,k_2}^{m_2}$ and $E_{c,k_2}^{M_2}$, expressed as

$$\begin{aligned} E_{c,k_2}^{m_2} &= \frac{M_2}{M_1}\left(E_{k_1} - B_2 - E_{k_2}\right) + \frac{m_2}{M_1} E_{c,k_1}^{M_1}, \\ E_{c,k_2}^{M_2} &= \frac{m_2}{M_1}\left(E_{k_1} - B_2 - E_{k_2}\right) + \frac{M_2}{M_1} E_{c,k_1}^{M_1}, \end{aligned} \quad (15)$$

are the energies carried by the secondary emitted particle m_2 and its residual nucleus M_2 from energy level E_{k_1} in the center-of-mass frame. E_{k_2} is the k_2th energy level of the residual nucleus M_2, and B_2 is binding energy of the m_2 particle in the residual nucleus M_1 (see Appendix B2).

In the case of the $(n, n\alpha)$ and $(n, 2\alpha)$ channels for the $n + {}^{12}\mathrm{C}$ reaction, the residual nuclei ${}^8\mathrm{Be}$ and ${}^5\mathrm{He}$ are very unstable and proceed spontaneously via two-body separation into m_3 and M_3 from the E_{k_2} level; for example, ${}^8\mathrm{Be} \rightarrow \alpha + \alpha$ and ${}^5\mathrm{He} \rightarrow n + \alpha$. The average energies of m_1 and m_2 expressed as Eqs. (9) and (13), and the average energies carried by two fraction particles (m_3 and M_3) in the laboratory frame can be obtained analytically by

$$\overline{E}_{m_3} = \frac{m_n m_3}{M_C^2} E_n + E_c^{m_3} - \frac{2m_3}{M_1 M_C}\sqrt{m_n m_1 E_n E_{c,k_1}^{m_1}}\, f_1^{m_1}, \quad (16)$$

and

$$\overline{E}_{M_3} = \frac{m_n M_3}{M_C^2} E_n + E_c^{M_3} - \frac{2M_3}{M_1 M_C}\sqrt{m_n m_1 E_n E_{c,k_1}^{m_1}}\, f_1^{m_1}. \quad (17)$$

Where m_3 and M_3 are masses of two clusters separated from M_2 at the E_{k_2} level, respectively. Here, $E_c^{m_3}$ and $E_c^{M_3}$, expressed as

$$\begin{aligned} E_c^{m_3} &= \frac{M_3}{M_2}(E_{k_2} + Q) + \frac{m_2 m_3}{M_1 M_2}\left(E_{k_1} - B_2 - E_{k_2}\right) \\ &\quad + \frac{m_3 m_1}{M_1 M_C}\left(E^* - B_1 - E_{k_1}\right), \\ E_c^{M_3} &= \frac{m_3}{M_2}\left(E_{k_2} + Q\right) + \frac{m_2 M_3}{M_1 M_2}\left(E_{k_1} - B_2 - E_{k_2}\right) \\ &\quad + \frac{M_3 m_1}{M_1 M_C}\left(E^* - B_1 - E_{k_1}\right), \end{aligned} \quad (18)$$

are the energies carried by two clusters separated with the Q value in the center-of-mass frame (see Appendix B3).

For the ${}^{12}\mathrm{C}(n,{}^5\mathrm{He}){}^8\mathrm{Be}$ channel, the ${}^5\mathrm{He}$ nucleus (denoted by m_1) separates spontaneously into m_a and m_b with $Q_2 = 0.894$ MeV, and ${}^8\mathrm{Be}$ (denoted by M_1) also does so into M_a and M_b with $Q_3 = 0.092$ MeV. The average energies carried by those four separate particles in the laboratory frame are expressed as

$$\overline{E}_{m_a} = \frac{m_n m_a}{M_C^2} E_n + E_c^{m_a} - \frac{2m_a}{m_1 M_C}\sqrt{m_n M_1 E_n E_{c,k_1}^{M_1}}\, f_1^{M_1}, \quad (19)$$

$$\overline{E}_{m_b} = \frac{m_n m_b}{M_C^2} E_n + E_c^{m_b} - \frac{2m_b}{m_1 M_C}\sqrt{m_n M_1 E_n E_{c,k_1}^{M_1}}\, f_1^{M_1}, \quad (20)$$

$$\overline{E}_{M_a} = \frac{m_n M_a}{M_C^2} E_n + E_c^{M_a} - \frac{2M_a}{M_1 M_C}\sqrt{m_n m_1 E_n E_{c,k_1}^{m_1}}\, f_1^{m_1}, \quad (21)$$

and

$$\overline{E}_{M_b} = \frac{m_n M_b}{M_C^2} E_n + E_c^{M_b} - \frac{2M_b}{M_1 M_C}\sqrt{m_n m_1 E_n E_{c,k_1}^{m_1}}\, f_1^{m_1}, \quad (22)$$

where

$$\begin{aligned} E_c^{m_a} &= \frac{m_b}{m_1}\left(E_{k_1(m_1)} + Q_2\right) + \frac{m_a}{m_1} E_{c,k_1}^{m_1}, \\ E_c^{m_b} &= \frac{m_a}{m_1}\left(E_{k_1(m_1)} + Q_2\right) + \frac{m_b}{m_1} E_{c,k_1}^{m_1}, \\ E_c^{M_a} &= \frac{M_b}{M_1}\left(E_{k_1(M_1)} + Q_3\right) + \frac{M_a}{M_1} E_{c,k_1}^{M_1}, \\ E_c^{M_b} &= \frac{M_a}{M_1}\left(E_{k_1(M_1)} + Q_3\right) + \frac{M_b}{M_1} E_{c,k_1}^{M_1}, \end{aligned} \quad (23)$$

are the energies carried by m_a, m_b, M_a, and M_b in the center-of-mass frame, respectively. $E_{k_1(m_1,M_1)}$ is the k_1th energy level of m_1 or M_1 (see Appendix B2).

B. For the $n + {}^{16}\mathrm{O}$ reaction

The information on the $n + {}^{16}\mathrm{O}$ reactions is listed in detail in Table II, at incident neutron energy E_n up to 30 MeV. For the reaction channels from the 1st to the 17th (except the 8th channel), the average energies carried by the emitted particles and their residual nuclei are in accord with the expressions given above from Eqs. (8)–(15). For the 18th–21st channels, the average energies in the laboratory frame carried by the third emitted particle m_3 and their residual nuclei M_3 are

TABLE II. Same as Table I, but for the $n + {}^{16}\mathrm{O}$ reaction at $E_n \leqslant 30$ MeV. Note: the (n, n') channel includes the elastic scattering channel ($E_{\mathrm{th}} = 0.0$).

No.	Channel	B	Q	E_{th}
1	(n, γ)	0.000	4.143	0.000
2	(n, n')	4.143	0.000	6.050
3	(n, p)	13.780	−9.637	10.245
4	(n, α)	6.358	−2.215	2.355
5	(n, d)	14.046	−9.903	10.528
6	(n, t)	18.622	−14.479	15.392
7	$(n,{}^3\mathrm{He})$	18.760	−14.617	15.539
8	$(n,{}^5\mathrm{He})$	12.199	−8.056	8.564
9	$(n,{}^6\mathrm{Li})$	23.561	−19.42	20.644
10	$(n, 2n)$	15.663	−15.663	16.651
11	(n, np)	12.127	−12.127	12.892
12	$(n, n\alpha)$	7.161	−7.161	7.613
13	(n, nd)	20.736	−20.736	22.044
14	(n, pn)	2.490	−12.127	12.892
15	$(n, \alpha\mathrm{n})$	4.946	−7.161	7.613
16	$(n, 2\alpha)$	10.646	−12.861	13.672
17	(n, dn)	10.833	−20.736	22.044
18	$(n, 2np)$	7.297	−22.960	24.408
19	(n, npn)	10.833	−22.960	24.408
20	$(n, p2n)$	10.833	−22.960	24.408
21	$(n, n2\alpha)$	1.665	−14.526	15.442

expressed as

$$\overline{E}_{m_3} = \frac{m_n m_3}{M_C^2} E_n + \frac{M_3}{M_2}\left(E_{k_2} - B_3 - E_{k_3}\right) + \frac{m_3}{M_2} E_{c,k_2}^{M_2} - \frac{2m_3}{M_C M_1}\sqrt{m_n E_n M_1 E_{c,k_1}^{M_1}}\, f_1^{m_1}, \tag{24}$$

and

$$\overline{E}_{M_3} = \frac{m_n M_3}{M_C^2} E_n + \frac{m_3}{M_2}\left(E_{k_2} - B_3 - E_{k_3}\right) + \frac{M_3}{M_2} E_{c,k_2}^{M_2} - \frac{2M_3}{M_C M_1}\sqrt{m_n E_n M_1 E_{c,k_1}^{M_1}}\, f_1^{m_1}. \tag{25}$$

The energies of m_3 and M_3 can be expressed in the center-of-mass frame as

$$E_{c,k_3}^{m_3} = \frac{M_3}{M_2}\left(E_{k_2} - B_3 - E_{k_3}\right) + \frac{m_3}{M_2} E_{c,k_2}^{M_2},$$
$$E_{c,k_3}^{M_3} = \frac{m_3}{M_2}\left(E_{k_2} - B_3 - E_{k_3}\right) + \frac{M_3}{M_2} E_{c,k_2}^{M_2}, \tag{26}$$

where E_{k_3} is the k_3th energy level of the residual nucleus M_3, and B_3 is the bounding energy of m_3 in residual nucleus M_2. $E_{c,k_1}^{M_1}$ and $E_{c,k_2}^{M_2}$ are expressed as Eqs. (11) and (15), respectively (see Appendix B3).

A special case is the residual nucleus ${}^8\mathrm{Be}$ in the reaction channel $(n, n2\alpha)$ which decays via two-body separation into two α particles with $Q_3 = 0.092$ MeV as mentioned above in the case of the E_{k_3} energy level. Here, the average energies carried by two α particles (denoted by m_4) can be expressed as (see Appendix B3)

$$\overline{E}_{m_4} = \frac{m_n m_4}{M_C^2} E_n + \frac{m_4}{M_3}\left(E_{k_3} + Q_3\right) + \frac{m_4}{M_3} E_{c,k_3}^{M_3} - \frac{2m_4}{M_C M_1}\sqrt{m_n E_n M_1 E_{c,k_1}^{M_1}}\, f_1^{m_1}. \tag{27}$$

For the $(n,{}^5\mathrm{He})$ channel, the first emitted particle is ${}^5\mathrm{He}$, which can separate spontaneously into a neutron and an α particle with $Q_2 = 0.894$ MeV. If the excited energy level of the residual nucleus ${}^{12}\mathrm{C}$ is too low to emit any particle, this decay contributes to the $(n, n\alpha)$ channel. The average energies in the laboratory frame carried by emitted particles can be obtained from Eqs. (19) and (20). If the energy level of the excited residual ${}^{12}\mathrm{C}$ is high enough to emit an α particle, this decay belongs with the $(n, n2\alpha)$ channel, and the average energies in the laboratory frame carried by all emitted particles can be obtained from Eqs. (24) and (27).

Obviously, the total energy through sequential emission reads in the laboratory frame as

$$\overline{E}_{\mathrm{total}} = \sum_i^{i_{\max}} \overline{E}_{m_i} + \overline{E}_{M_{i_{\max}}} + E_{k_{i_{\max}}} = E_n + B_n - \sum_i^{i_{\max}} B_i, \tag{28}$$

where $\overline{E}_{m_i}$ is the average energy carried by the ith ejectile, and $\overline{E}_{M_{i_{\max}}}$ is the average energy carried by the last residual nucleus. Therefore, the energy balance holds exactly. For two-body separation, $Q = -B$, and the energy balance again holds.

IV. RESULTS

A. Partial kerma coefficients

The partial kerma coefficients of the various secondary charged particles below 30 MeV according to formula (4) for carbon and oxygen are given in Figs. 1 and 2, respectively. The calculations of this paper describe well the experimental and extrapolated kerma coefficients for α, proton, deuteron, and tritium. Unfortunately, the experimental partial kerma coefficients are too sparse below 30 MeV. Experimental data (open triangles) of Ref. [31] at 27.4 MeV are not corrected for the contributions from the ejectile energies below the experimental low-energy cuts in the measured spectra, as mentioned in Ref. [4]. Therefore, the extrapolated partial kerma coefficients (full dots) down to the thresholds are experimental in the sense that no theoretical concept was used in their determination [4].

Figures 1 and 2 show that the α-particle contribution to the total kerma coefficients is dominated by the large α-particle production cross sections for both carbon and oxygen below 30 MeV. The proton contribution to the total kerma coefficients increases with neutron incident energy. The present calculated results (continuous line) in the energy range from threshold to 30 MeV are compared with the values (dashed line) evaluated by Chadwick [9] only from 20 to 30 MeV for α, proton, and deuteron. The results of tritium, ${}^3\mathrm{He}$, and ${}^6\mathrm{Li}$ are provided, too, in Figs. 1 and 2, although their contributions to the total kerma coefficients are small.

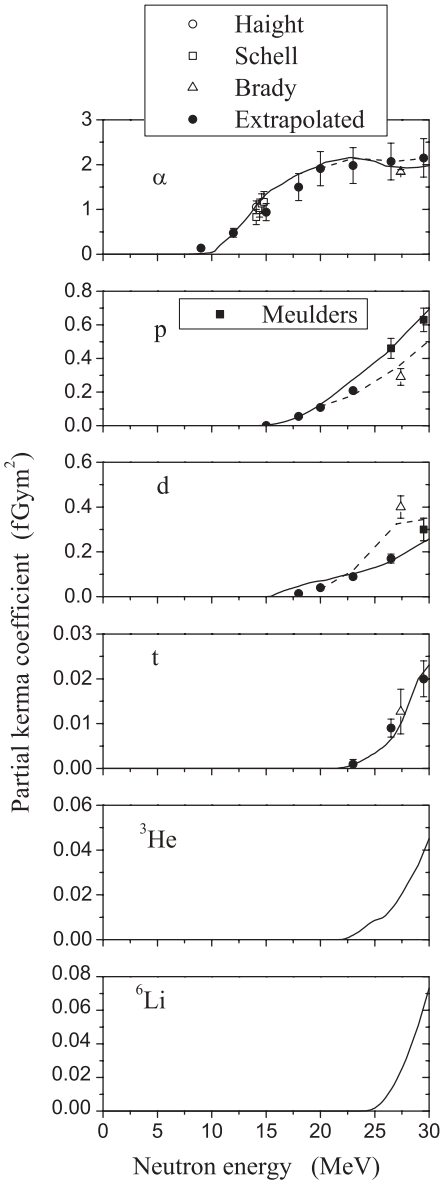

FIG. 1. Partial kerma coefficients of this work (continuous line) for carbon vs the neutron energies for α, proton, deuteron, tritium, ^{3}He, and ^{6}Li. Experimental data (see legend) are derived from Refs. [4,29–31], and the extrapolated data are from Ref. [4]. Theoretical calculations of Ref. [9] are also shown (dashed line).

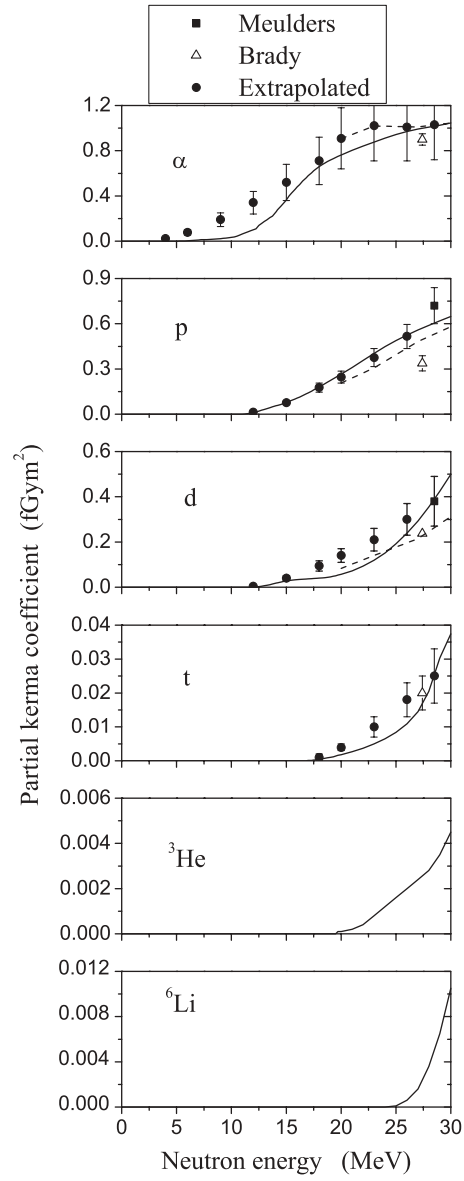

FIG. 2. Same as Fig. 1, but for oxygen.

B. Elastic recoil kerma coefficients

In terms of formulas (4), (10), and (11), where m_1 and M_1 are the masses of neutron and target nucleus, the elastic recoil kerma coefficients are expressed easily as

$$k_{\Phi}^{\mathrm{el}} = N\frac{2m_0M_1E_n}{M_0^2}\left(1 - f_1^{m_1}\right)\sigma_{\mathrm{el}}, \tag{29}$$

where σ_{el} is the elastic cross section, and $f_1^{m_1}$ is the first Legendre coefficient of elastic angular distribution. The optical model calculation can obtain the cross section of the total and elastic scattering as a smooth curve only, but the experimental and evaluated cross sections show a lot of structure. So the elastic cross sections σ_{el} and their first Legendre coefficient $f_1^{m_1}$ in formula (29) were derived from EBDF/B-VII-b3, in which the elastic cross sections and the elastic angular distributions agree very well with the experimental data. It should be noted that the elastic angular distribution (MF = 4, MT = 2) for carbon is tabulated in EBDF/B-VIIb3 at high incident energy range (>20 MeV), so their first Legendre coefficients in this paper at high neutron energy (20–30 MeV) are obtained by fitting the elastic angular distribution experimental data. The elastic recoil kerma coefficients calculated according to formula (29) (continuous line) are shown in Fig. 3 for carbon and oxygen. The calculated results of this paper are in good agreement with the experimental data. The elastic recoil kerma coefficients at low neutron energies (<20 MeV) show variations corresponding to resonances in the elastic cross section. However, the elastic recoil kerma coefficients decrease slowly with incident neutron energy, because the

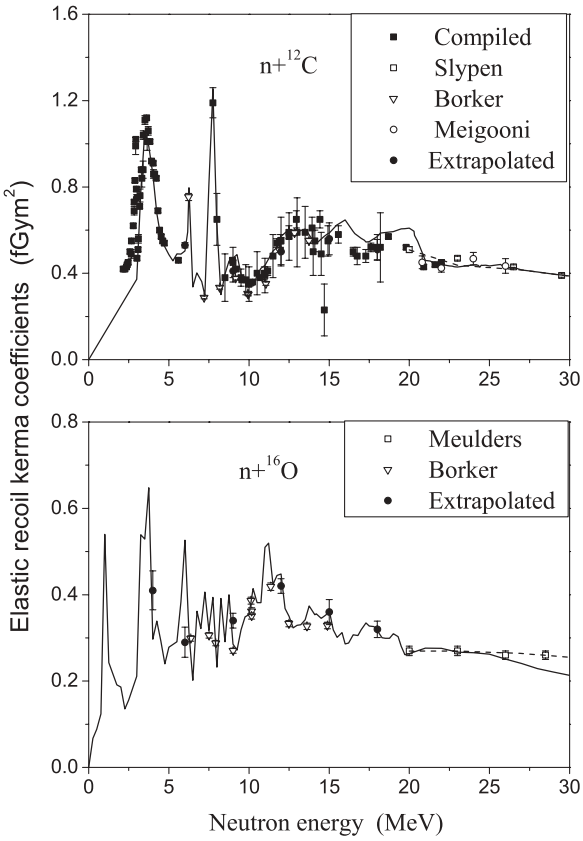

FIG. 3. Elastic recoil kerma coefficients of this work (continuous line) for carbon and oxygen vs neutron energies. Theoretical calculations of Ref. [9] are shown (dash line). In the carbon panel, the experimental data shown as full squares were compiled by Slypen in Table 3 of Ref. [32], and other experimental data (see legend) are derived from Refs. [4,32–34], the extrapolated elastic recoil data are from Ref. [4]. In the oxygen panel, the experimental data are derived from Refs. [4,33], and the extrapolated elastic recoil data are again from Ref. [4].

elastic angular distribution becomes more forward peaked and the elastic scattering cross section decreases at high energies (>20 MeV). In Fig. 3, the model calculation (dashed line) of Ref. [9] is shown only for the neutron energy region of 20–30 MeV.

C. Total kerma coefficients

The calculated total kerma coefficients of this work (full line) and the experimental data for carbon and oxygen are given in Figs. 4 and 5, respectively, below 30 MeV. The comparisons between the model calculation of this work and the result (dashed line) derived from Table II of Ref. [9], which is obtained by the NJOY data processing code, are also shown. The results of this work and Ref. [9] are generally in quite good agreement with the measurements. Though the spread in the measured values is large, the deviations between the calculations and measurements are generally within the uncertainties of the kerma coefficients. As shown in Fig. 4,

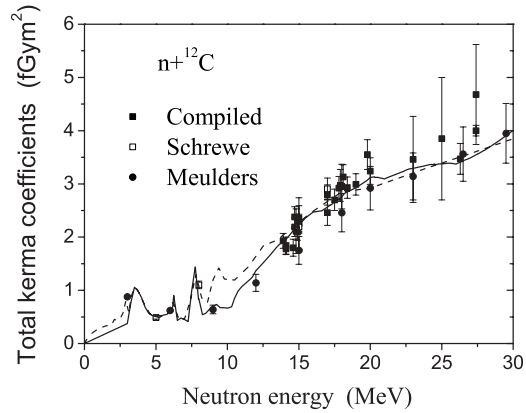

FIG. 4. Total kerma coefficients for carbon vs neutron energies. The experimental data shown as full squares were compiled by Broerse in Ref. [35], and the other experimental data (open squares, full dots) are derived from Refs. [2,4], respectively. The evaluated results of Ref. [9] are shown as the dashed line.

there is some discrepancy between the calculation of this work and the results of Ref. [9] from 8 to 15 MeV and below 3 MeV. The results of this work seem more reasonable for carbon. In the ENDF/B-VIIb3 library, the inelastic scattering channel corresponding to γ-ray excited levels of ^{12}C are included MT = 51–57 (real levels), MT = 58–62 (pseudo levels), and MT = 91 (continuous state level). In this model calculation, only the first two excited levels of ^{12}C purely belong to the inelastic scattering channel, and the α emission and γ decay from the third excited level competes with each other. All the residual nucleus states are discrete levels with no continuum.

However, as shown in Fig. 5 for oxygen, the present work underestimates the total kerma coefficients in the 6–20 MeV region of neutron energy, and overestimates them above 20 MeV. The evaluation of Ref. [9] gets opposite results compared to this work in the above two regions. We think that the discrepancies between this work and Ref. [9] are

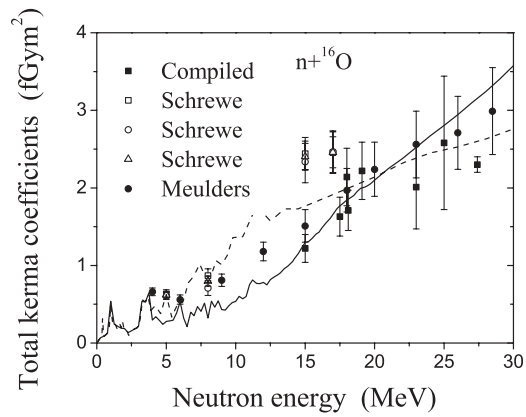

FIG. 5. Total kerma coefficients for oxygen vs neutron energies. The compiled experimental data are from Broerse [35]. The three Schrewe experimental data sets (see legend) are derived from different oxides in Ref. [2], and the residual data (full dots) are from Ref. [4]. The evaluated results of Ref. [9] are also shown (dashed line).

attributable to the different way of processing the inelastic scattering channel. In the ENDF/B-VIIb3 library (this new version for oxygen has some improvement on inelastic scattering vs earlier versions, such as ENDF/B-VI and so on), the inelastic reaction channel corresponding to γ-emitting excited levels of ^{16}O are included MT = 51–57 (the 1st–5th, 9th, and 10th excited levels) and MT = 91 (continuous state level). The 6th–8th excited levels are omitted because they decay primarily by α-particle emission, therefore those data are included in the (n, α) channel. The result of MT = 91 based on GNASH calculations from threshold to 30 MeV is adjusted such that the difference between total and nonelastic cross sections agrees with elastic cross section measurements. In this work, the pure inelastic scattering channel corresponding to γ-emitting excited levels include the 1st–5th, 9th, 10th, and 12th excited levels. The 6th–8th, 11th, and 13th–17th excited levels can emit an α, therefore their contributions are included in the $(n, n\alpha)$ channel. The 18th excited level can emit a proton and contribute to the (n, np) channel. The 19th and higher excited levels can emit several light particles, including neutron, proton, α, deuteron, and tritium, so their contributions belong in the $(n, 2n)$, (n, np), (n, nd), and $(n, n\alpha)$ channels, respectively. The discrepancies between the model calculations and the experimental data indicate that the way of processing inelastic channels must be improved further in detail.

V. SUMMARY

A new calculation formula for the kerma coefficient, based on the statistical theory of neutron-induced light nucleus reactions, has been developed in this paper. For $n + {}^{12}$C and $n + {}^{16}$O reactions, the channels are analyzed below 30 MeV and the recoil effects are exactly taken into account in all reaction processes. The optical model parameters of the neutron and all emitted particles, which can reproduce very well the outgoing neutron double-differential cross sections, are adopted for $n + {}^{12}$C and $n + {}^{16}$O reactions. Two new sets of partial, elastic recoil, and total kerma coefficients for carbon and oxygen calculated according to Eq. (4) are consistent with existing experimental kerma coefficient data. To reproduce the resonant structure of elastic recoil kerma coefficients, the elastic cross sections and their first Legendre coefficients are derived from EBDF/B-VIIb3. The discrepancies of the total kerma coefficients between the experimental data and the evaluation results for oxygen have been further discussed, and we will attempt to improve them in the future. Furthermore, a more extensive region of incident neutron energy will be studied in the future, and the kerma coefficients of some radiobiologically important substances will be deduced.

ACKNOWLEDGMENTS

This work was supported by the National Natural Science Foundation of China under Grant No. 10547005.

APPENDIX A: DYNAMICS OF THE NEUTRON-INDUCED LIGHT NUCLEUS REACTION

For light target elements that have few nucleons, statistical equilibrium is unlikely to be attained below 30 MeV through multiple collisions before particle emission. Hence the preequilibrium reaction mechanism dominates the reaction processes. Furthermore, the corresponding residual nuclides always end up in discrete levels after particle emission. These discrete levels have individual spins and parities which effect different particle emissions. To deal with the above problems, an attempt at describing the neutron-induced light nucleus reaction [10] was carried out with the united Hauser-Feshbach and exciton model [36]. Fortunately, these efforts were successful. The statistical theory of neutron-induced light nucleus reaction has been developed, and the outgoing neutron double-differential cross section can be reproduced very well with the experimental data for such different targets as ^{6}Li [15], ^{7}Li [16], ^{10}B [17], ^{11}B [18], ^{12}C [19], ^{14}N [20], ^{16}O [21], and ^{19}F [22].

In terms of this statistical theory, the energy spectrum, angular distribution, and double-differential cross section can be analytically expressed after considering the conservation of energy, angular momentum, and parity in the emission processes from the discrete levels of the compound nucleus to the discrete levels of the residual nuclei. For example, the formula for the energy spectrum reads as follows [36]:

$$\frac{d\sigma}{d\varepsilon} = \sum_{j\pi} \sigma_a^{j\pi} \sum_n P^{j\pi}(n) \frac{W_b^{j\pi}(n, E^*, \varepsilon)}{W_T^{j\pi}(n, E^*)}, \tag{A1}$$

where j and π represent the angular momentum and the parity, respectively, and $\sigma_a^{j\pi}$ is the absorption cross section of the $j\pi$ channel, derived from the phenomenological spherical optical potential model. $W_b^{j\pi}(n, E^*, \varepsilon)$ is the emission rate of particle b at the n-exciton state in the $j\pi$ channel with outgoing energy ε. $W_T^{j\pi}(n, E^*)$ is the total emission rate of the n-exciton state in the $j\pi$ channel, and E^* stands for excitation energy. $P^{j\pi}(n)$ is the occupation probability at the n-exciton state in the $j\pi$ channel. If the parity and angular momentum effects are not considered, the theory is reduced to the exciton model [11]. Whereas if the preequilibrium effect is omitted, it is reduced to the Hauser-Feshbach model [12].

The calculated results show that only the first few exciton numbers ($n_0 = 3$ or 5) must be considered in the preequilibrium process for a light nucleus reaction. So Eq. (A1) can be analytically expressed as

$$\frac{d\sigma}{d\varepsilon} = \sum_{j\pi} \sigma_a^{j\pi} \left\{ \sum_{n=3}^{n_0} P^{j\pi}(n) \frac{W_b^{j\pi}(n, E^*, \varepsilon)}{W_T^{j\pi}(n, E^*)} + Q^{j\pi} \frac{W_b^{j\pi}(E^*, \varepsilon)}{W_T^{j\pi}(E^*)} \right\}, \tag{A2}$$

where $Q^{j\pi} = 1 - \sum_{n=3}^{n_0} P^{j\pi}(n)$ is the occupation probability of the equilibrium state. The first term of Eq. (A2) represents the preequilibrium emission, and the second is described by Hauser-Feshbach theory.

The occupation probability $P^{j\pi}(n)$ can be obtained by solving the $j\pi$-dependent exciton master equation as follows [27]:

$$\frac{d}{dt}P^{j\pi}(n,t) = \lambda_{n+2}^{j\pi-}P^{j\pi}(n+2,t) + \lambda_{n-2}^{j\pi+}P^{j\pi}(n-2,t) - \left[\lambda_n^{j\pi+} + \lambda_n^{j\pi-} + W_T^{j\pi}(n,E^*)\right]P^{j\pi}(n,t), \tag{A3}$$

where $\lambda_n^{j\pi\pm}$ stands for the internal transition rate of the n-exciton state to the $(n+2)$- and $(n-2)$-exciton states in the $j\pi$ channel. For the light nucleus reaction, while the exciton number n is small (for example, $n_0 = 3$), there is an approximate expression $\lambda_n^{j\pi+} \approx W_T^{j\pi}(n) \gg \lambda_{n+2}^{j\pi-}$ that allows the occupation probability $P^{j\pi}(n_0)$ to be analytically obtained, as expressed in Ref. [27].

On the basis of the united Hauser-Feshbach and exciton model, after considering emission rates of the nucleon (neutron and proton) [37] and complex particle [28,38–40] in equilibrium and preequilibrium states, the expressions of the outgoing particle double-differential cross sections are obtained formally as

$$\frac{d^2\sigma}{d\varepsilon\, d\Omega} = \sum_n \frac{d\sigma(n)}{d\varepsilon}A(n,\varepsilon,\Omega), \tag{A4}$$

where $d\sigma(n)/d\varepsilon$ is the energy spectrum obtained by Eq. (A1) or (A2), and $A(n,\varepsilon,\Omega)$ is the angular factor as shown in Ref. [23] in detail for different particle emissions.

APPENDIX B: KINEMATICS OF THE NEUTRON-INDUCED LIGHT NUCLEUS REACTION

1. Single-particle emission process

For the (n,n), (n,n'), (n,p), (n,α), (n,d), (n,t), $(n,^3\mathrm{He})$, and $(n,^6\mathrm{Li})$ reaction channels listed in Tables I and II, the energies carried by the first emitted particle and its residual nucleus in the center-of-mass frame are given by Eq. (11). So the average energies in the laboratory frame are obtained by averaging the angular distribution [Eq. (12)] in the center-of-mass frame as

$$\begin{aligned}\overline{E}_{m_1} &= \int \frac{1}{2}m_1\left(\vec{V}_c^{\,M_C} + \vec{v}_c^{\,m_1}\right)^2 \frac{d\sigma}{d\Omega_c^{m_1}}\, d\Omega_c^{m_1} \\ &= \sum_l \int \frac{1}{2}m_1\left[\left(V_c^{M_C}\right)^2 + \left(v_c^{m_1}\right)^2 + 2V_c^{M_C}\, v_c^{m_1}\cos\theta_c^{m_1}\right] \\ &\quad \times \frac{2l+1}{4\pi} f_l^{m_1} P_l\left(\cos\theta_c^{m_1}\right) d\Omega_c^{m_1} \\ &= \frac{m_n m_1}{M_C^2}E_n + E_{c,K_1}^{m_1} + 2\frac{\sqrt{m_n m_1 E_n E_{c,K_1}^{m_1}}}{M_C} f_1^{m_1},\end{aligned} \tag{B1}$$

where $\vec{V}_c^{\,M_C}$ is the velocity of the compound mass center, and $\vec{v}_c^{\,m_1}$ is the velocity of the emitted particle in the center of mass. The orthogonality of the Legendre polynomials is used in the above operation. A similar operation is carried out for the residual nuclide M_1, and the same expression of Eq. (10) is obtained.

2. Secondary-particle emission process

When the secondary particle m_2 is emitted by M_1 from energy level E_{k_1} and the residual nuclide M_2 stays in the E_{k_2} level, such as channels 10–19 in Table I and 10–17 in Table II, the energies carried by the secondary emitted particle m_2 and its residual nucleus M_2 in the residual nuclear coordinate system (denoted by the subscript r) are expressed as

$$\begin{aligned}\varepsilon_r^{m_2} &= \frac{M_2}{M_1}\left(E_{k_1} - B_2 - E_{k_2}\right), \\ E_r^{M_2} &= \frac{m_2}{M_1}\left(E_{k_1} - B_2 - E_{k_2}\right).\end{aligned} \tag{B2}$$

Attention is paid to the fact that the first residual nuclide M_1 is recoiling in the center-of-mass frame when it emits the secondary particle m_2. But in the residual nuclear coordinate system, the energies of m_2 and M_2 are definite, as shown in Eq. (B2).

From the velocity relation of m_2 and M_1 between the center-of-mass frame and the residual nuclear coordinate system, $\vec{v}_c^{\,m_2} = \vec{V}_c^{\,M_1} + \vec{v}_r^{\,m_2}$ (as shown in Fig. 6), one can obtain the angular formula and extreme energy of m_2 in the center-of-mass frame as follows:

$$\cos\Theta = \frac{\varepsilon_c^{m_2}/\varepsilon_r^{m_2} - 1 - \gamma^2}{2\gamma} = \sqrt{\frac{\varepsilon_c^{m_2}}{\varepsilon_r^{m_2}}}\cos\theta - \gamma, \tag{B3}$$

and

$$\varepsilon_c^{m_2,\max} = \varepsilon_r^{m_2}(1+\gamma)^2, \quad \varepsilon_c^{m_2,\min} = \varepsilon_r^{m_2}(1-\gamma)^2, \tag{B4}$$

where Θ is the angle between $\vec{v}_r^{\,m_2}$ and $\vec{V}_c^{\,M_1}$, θ is the angle between $\vec{v}_c^{\,m_2}$ and $\vec{V}_c^{\,M_1}$, and $\gamma = \frac{V_c^{M_1}}{v_r^{m_2}} = \sqrt{\frac{m_2 E_c^{M_1}}{M_1 \varepsilon_r^{m_2}}}$ is an important quantity that embodies the influence of the recoiling nuclide on the subsequent emission. A simple approximate method was assumed whereby the recoiling nuclide stays stationary (i.e., $\gamma = 0$) in the earlier studies. Obviously, although the energy of m_2 in the residual nuclear coordinate system is single-valued, the energy in the center-of-mass frame is continuous, i.e., $\varepsilon_c^{m_2,\min} \leqslant \varepsilon_c^{m_2} \leqslant \varepsilon_c^{m_2,\max}$. So the multisequential emission must be described by the double-differential cross section in the center-of-mass frame.

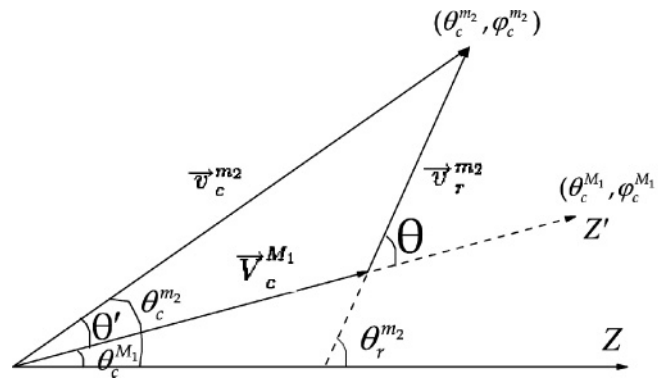

FIG. 6. Velocity vector relation of m_2 and M_1 between the center-of-mass frame and the residual nuclear coordinate system.

In the residual nuclear coordinate system, the emitted energy is single-valued according to Eq. (B2), so the double-differential cross section can be approximately expressed as

$$\frac{d^2\sigma}{d\varepsilon_r^{m_2}\,d\Omega_r^{m_2}} = \frac{1}{4\pi}\delta\left[\varepsilon_c^{m_2} - \varepsilon_r^{m_2}\left(1 + 2\gamma\cos\Theta + \gamma^2\right)\right]. \quad \text{(B5)}$$

The double-differential cross section of the secondary emitted particle m_2 in the center-of-mass frame can be obtained by averaging the angular distribution [Eq. (12)] of the first residual nuclide M_1 through tediously complicated mathematical calculations [10]:

$$\begin{aligned}\frac{d^2\sigma}{d\varepsilon_c^{m_2}\,d\Omega_c^{m_2}} &= \int d\Omega_c^{M_1}\frac{d\sigma}{d\Omega_c^{M_1}}\sqrt{\frac{\varepsilon_c^{m_2}}{\varepsilon_r^{m_2}}}\frac{d^2\sigma}{d\varepsilon_r^{m_2}d\Omega_r^{m_2}} \\ &= \sum_l \frac{(-1)^l}{16\pi\gamma\varepsilon_r^{m_2}}(2l+1)f_l^{m_1}P_l(\eta)P_l\left(\cos\theta_c^{m_2}\right),\end{aligned} \quad \text{(B6)}$$

where $\eta = \sqrt{\varepsilon_r^{m_2}/\varepsilon_c^{m_2}}\,\frac{\varepsilon_c^{m_2}/\varepsilon_r^{m_2}-1+\gamma^2}{2\gamma}$, and $\sqrt{\varepsilon_c^{m_2}/\varepsilon_r^{m_2}}$ is a Jacobian factor. Adopting the recommended format of Ref. [26], the double-differential cross section in the center-of-mass frame can be also expressed as

$$\frac{d^2\sigma}{d\varepsilon_c^{m_2}\,d\Omega_c^{m_2}} = \frac{1}{4\pi}\sum_l(2l+1)f_l^{m_2}P_l\left(\cos\theta_c^{m_2}\right). \quad \text{(B7)}$$

The Legendre coefficients of m_1 and m_2 are related such that

$$f_l^{m_2} = \frac{(-1)^l}{4\gamma\varepsilon_r^{m_2}}f_l^{m_1}P_l(\eta). \quad \text{(B8)}$$

In the center-of-mass frame, the emitted energy $E_{c,k_2}^{m_2}$ of the secondary particle is obtained by averaging the double-differential cross section:

$$\begin{aligned}E_{c,k_2}^{m_2} &= \int_{\varepsilon_c^{m_2,\min}}^{\varepsilon_c^{m_2,\max}}\varepsilon_c^{m_2}\frac{d^2\sigma}{d\varepsilon_c^{m_2}d\Omega_c^{m_2}}d\varepsilon_c^{m_2}d\Omega_c^{m_2} \\ &= \int_{\varepsilon_c^{m_2,\min}}^{\varepsilon_c^{m_2,\max}}\varepsilon_c^{m_2}f_0^{m_2}d\varepsilon_c^{m_2} \\ &= \frac{M_2}{M_1}(E_{k_1} - B_2 - E_{k_2}) + \frac{m_2}{M_1}E_{c,k_1}^{M_1}.\end{aligned} \quad \text{(B9)}$$

In the laboratory frame, the secondary-particle energy $\overline{E}_{m_2}$ can also be obtained by averaging the double-differential cross section in the center-of-mass frame as

$$\begin{aligned}\overline{E}_{m_2} &= \int\frac{1}{2}m_2\left(\overrightarrow{V}_c^{M_1} + \overrightarrow{v}_c^{m_2}\right)^2\frac{d^2\sigma}{d\varepsilon_c^{m_2}\,d\Omega_c^{m_2}}\,d\varepsilon_c^{m_2}\,d\Omega_c^{m_2} \\ &= \frac{m_n m_2 E_n}{M_C} + E_{c,k_2}^{m_2} + 2\int_{\varepsilon_c^{m_2,\min}}^{\varepsilon_c^{m_2,\max}}\frac{\sqrt{m_n m_2 E_n\varepsilon_c^{m_2}}}{M_C}f_1^{m_2}\,d\varepsilon_c^{m_2} \\ &= \frac{m_n m_2 E_n}{M_C} + E_{c,k_2}^{m_2} - 2\frac{m_2}{M_C}\sqrt{\frac{m_n E_n E_{c,k_1}^{M_1}}{M_1}}f_1^{m_1}.\end{aligned} \quad \text{(B10)}$$

Using linear momentum conservation in the center-of-mass frame, the formula $M_1E_{c,k_1}^{M_1} = m_1E_{c,k_1}^{m_1}$ can be derived, and the same expression between Eqs. (13) and (B10) is also easily obtained. As shown in Eq. (B10), a third term accounts for the recoiling effect of the residual nuclide.

The same operation for the secondary residual nuclide M_2 is carried out merely by exchanging m_2 with M_2 in the above listed formulas. So formula (14) can be easily obtained, although the process is tedious and complex.

The formulas (13) and (14), including the $f_1^{m_1}$ term, show a clear recoiling effect. However, in the center-of-mass frame, the angular distribution of the emitted particle, described by Hauser-Feshbach equilibrium state theory, is symmetrical about 90° and there is no $l = 1$ partial wave [12]. The larger the $f_1^{m_1}$, the stronger the recoil effect. This is one of the most important features of the neutron-induced light nucleus reaction. Certainly, it requires that enough partial waves be included to properly describe the double-differential cross section, but only the $l = 1$ partial wave can maintain energy conservation through the statistical averaging method.

Specially, for the ^{12}C$(n,^5$He$)^8$Be channel, the ^{5}He nucleus (denoted by m_1) separates spontaneously into m_a and m_b with $Q_2 = 0.894$ MeV; and ^{8}Be (denoted by M_1) does the same, into M_a and M_b with $Q_3 = 0.092$ MeV. The average energy carried by $m_{a,b}$ and $M_{a,b}$ can be obtained through an analogous method to that in Appendix B2.

For $m_{a,b}$ particles, M_1 can be regarded as the first emitted particle, and its residual nuclide is m_1, which can spontaneously emit $m_{a,b}$ particles. So Eq. (B2) is substituted by the formulas

$$\varepsilon_r^{m_a} = \frac{m_b}{m_1}Q_2, \quad \varepsilon_r^{m_b} = \frac{m_a}{m_1}Q_2. \quad \text{(B11)}$$

The same straightforward operation as in Appendix B2 is performed, and the same results as formulas (19) and (20) are obtained.

Similarly, for $M_{a,b}$ particles, m_1 can be regarded as the first emitted particle, and its residual nuclide is M_1, which can spontaneously emit $M_{a,b}$ particles. So Eq. (B2) is replaced by the formulas

$$\varepsilon_r^{M_a} = \frac{M_b}{M_1}Q_3, \quad \varepsilon_r^{M_b} = \frac{M_a}{M_1}Q_3. \quad \text{(B12)}$$

The same straightforward operation as in Appendix B2 is performed, and the same results as in formulas (21) and (22) are obtained.

3. Multisequential-particle emission process

After secondary-particle emission, the residual nuclide M_2 is unstable and can separate spontaneously [as in the ^{12}C$(n,n\alpha)^8$Be and ^{12}C$(n,2\alpha)^5$He channels] or emit two particles (such as in the 18th–21st channels in Table II). The emitted energies of m_3 and M_3 in the residual nuclear coordinate are expressed as

$$\varepsilon_r^{m_3} = \frac{M_3}{M_2}\left(Q_{\text{cluster}} + E_{k_2}\right), \quad E_r^{M_3} = \frac{m_3}{M_2}\left(Q_{\text{cluster}} + E_{k_2}\right), \quad \text{(B13)}$$

or

$$\varepsilon_r^{m_3} = \frac{M_3}{M_2}\left(E_{k_2} - B_3 - E_{k_3}\right), \quad E_r^{M_3} = \frac{m_3}{M_2}\left(E_{k_2} - B_3 - E_{k_3}\right), \quad \text{(B14)}$$

where Q_{cluster} is the reaction Q value of two-body separation, and E_{k_3} is the level of the residual nucleus M_3.

With definitions similar to those in Appendix B2, i.e.,

$$\gamma_3 = \sqrt{\frac{m_3 E_{c,k_2}^{M_2}}{M_2 \varepsilon_r^{m_3}}}, \quad \eta_3 = \sqrt{\frac{\varepsilon_r^{m_3}}{E_c^{m_3}}} \frac{E_c^{m_3}/\varepsilon_r^{m_3} - 1 + \gamma_3^2}{2\gamma_3}, \tag{B15}$$

where the third emitted particle energy in the center-of-mass frame $E_c^{m_3}$ is not a single value, because $E_{c,k_2}^{M_2}$ is not single-valued. Thus γ_3 has a region expressed as [41]

$$\gamma_{3,\min} = \sqrt{\frac{m_3 E_{c,k_2}^{M_2,\min}}{M_2 \varepsilon_r^{m_3}}}, \quad \gamma_{3,\max} = \sqrt{\frac{m_3 E_{c,k_2}^{M_2,\max}}{M_2 \varepsilon_r^{m_3}}}. \tag{B16}$$

In the center-of-mass frame, the maximal energy $E_c^{m_3,\max}$ of the third emitted particle m_3, whose direction of motion ($\overrightarrow{v}_r^{m_3}$) in the residual nuclear coordinates is the same as the initial recoil direction of M_2($\overrightarrow{V}_c^{M_2}$) in the center-of-mass frame is expressed as

$$E_c^{m_3,\max} = \varepsilon_r^{m_3}(1 + \gamma_{3,\max})^2. \tag{B17}$$

However, when the directions of $\overrightarrow{v}_r^{m_3}$ and $\overrightarrow{V}_c^{M_2}$ are opposite, the minimal energy $E_c^{m_3,\min}$ of the third emitted particle m_3 in the center-of-mass frame has three states, i.e.,

$$E_c^{m_3,\min} = \begin{cases} \varepsilon_r^{m_3}(1 - \gamma_{3,\min})^2 & 1 \leqslant \gamma_{3,\min} \leqslant \gamma_{3,\max}, \\ 0 & \gamma_{3,\min} \leqslant 1 \leqslant \gamma_{3,\max}, \\ \varepsilon_r^{m_3}(1 - \gamma_{3,\max})^2 & \gamma_{3,\min} \leqslant \gamma_{3,\max} \leqslant 1. \end{cases} \tag{B18}$$

The double-differential cross section of the third emitted particle m_3 in the center-of-mass frame can also be expressed as

$$\frac{d^2\sigma}{d\varepsilon_c^{m_3} d\Omega_c^{m_3}} = \frac{1}{4\pi} \sum_l (2l+1) f_l^{m_3} P_l\left(\cos\theta_c^{m_3}\right). \tag{B19}$$

The same method as in Appendix B2 is used to obtain the relation between Legendre coefficients as

$$f_l^{m_3} = \frac{1}{4\gamma \varepsilon_r^{m_3}} f_l^{M_2} P_l(\eta_3). \tag{B20}$$

It is worth remembering that the $E_{c,k_2}^{M_2}$ is not a single value as mentioned above, so the Legendre coefficient $f_l^{M_2}(E_{c,E_{k_2}}^{M_2})$ is a continuous distribution. In terms of the statistical averaging law, the coefficient $f_l^{m_3}$ will be obtained by integrating Eq. (B20)

$$f_l^{m_3} = \int_{a_3}^{b_3} \frac{1}{4\gamma \varepsilon_r^{m_3}} f_l^{M_2} P_l(\eta_3)\, dE_{c,E_{k_2}}^{M_2}, \tag{B21}$$

where

$$a_3 = \max\left\{E_{c,E_{k_2}}^{M_2,\min}, \quad \frac{M_2}{m_3}\varepsilon_r^{m_3}\left(\sqrt{\varepsilon_c^{m_3}/\varepsilon_r^{m_3}} - 1\right)^2\right\}, \tag{B22}$$

$$b_3 = \min\left\{E_{c,E_{k_2}}^{M_2,\max}, \quad \frac{M_2}{m_3}\varepsilon_r^{m_3}\left(\sqrt{\varepsilon_c^{m_3}/\varepsilon_r^{m_3}} + 1\right)^2\right\},$$

are the maximal and minimal values of $E_{c,E_{k_2}}^{M_2}$, respectively.

In the center-of-mass frame, the third-particle emitted energy $E_c^{m_3}$ is obtained by averaging the double-differential cross section:

$$\begin{aligned} E_c^{m_3} &= \int_{\varepsilon_c^{m_3,\min}}^{\varepsilon_c^{m_3,\max}} \varepsilon_c^{m_3} \frac{d^2\sigma}{d\varepsilon_c^{m_3} d\Omega_c^{m_3}} d\varepsilon_c^{m_3}\, d\Omega_c^{m_3} \\ &= \int_{\varepsilon_c^{m_3,\min}}^{\varepsilon_c^{m_3,\max}} \varepsilon_c^{m_3} f_0^{m_3} d\varepsilon_c^{m_3} = \varepsilon_r^{m_3} + \frac{m_3}{M_2} E_{c,k_2}^{M_2}. \end{aligned} \tag{B23}$$

The velocity relation $\overrightarrow{v}_c^{m_3} = \overrightarrow{V}_c^{M_2} + \overrightarrow{v}_r^{m_3}$ and the technique of changing the variables of integration are adopted to obtain the result above.

In the laboratory frame, the third-particle energy $\overline{E}_{m_3}$ can be also obtained by averaging the double-differential cross section in the center-of-mass frame as follows:

$$\begin{aligned} \overline{E}_{m_3} &= \int \frac{1}{2} m_3 \left(\overrightarrow{V}_c^{M_2} + \overrightarrow{v}_c^{m_3}\right)^2 \frac{d^2\sigma}{d\varepsilon_c^{m_3} d\Omega_c^{m_3}} d\varepsilon_c^{m_3}\, d\Omega_c^{m_3} \\ &= \frac{m_3 m_n E_n}{M_C^2} + E_c^{m_3} - 2\frac{m_3}{M_C}\sqrt{\frac{m_n E_n E_{c,k_1}^{M_1}}{M_1}} f_1^{m_1}. \end{aligned} \tag{B24}$$

The same operation for the residual nuclide M_3 is carried out simply by exchanging m_3 with M_3 in the formulas above. When the residual nucleus M_3 can emit smaller particles or separate spontaneously into two clusters (denoted by m_4 and M_4), such as in the ^{16}O$(n, n2\alpha)^8$Be channel in Table II, the expressions for the energies of m_4 and M_4 in the center-of-mass and laboratory frames can be obtained as Eq. (27) using the above method.

[1] *ICRU Report No. 63, Nuclear Data for Neutron and Proton Radiotherapy and for Radiation Protection* (International Commission on Radiation Units and Measurements, Bethesda, MD, 2000).

[2] U. J. Schrewe, W. D. Newhauser, H. J. Brede, and P. M. DeLuca, Jr., Phys. Med. Biol. **45**, 651 (2000).

[3] J. Blomgren and N. Olsson, Radiat. Prot. Dosim. **103**, 293 (2003).

[4] J. P. Meulders, S. Benck, and I. Slypen *et al.*, Med. Phys. **27**, 2541 (2000).

[5] I. Slypen, S. Benck, J. P. Meulders, and V. Corcalciuc, Phys. Med. Biol. **45**, 577 (2000).

[6] R. E. MacFarlane, The NJOY Nuclear Data Processing System, Version 91 (Los Alamos National Laboratory, Los Alamos, NM, 1994).

[7] Li zhang and M. A. Abdo, Fusion Eng. Des. **36**, 479 (1997).

[8] Zhenzhou Liu and Jinxiang Chen, J. Radiol. Prot. **28**, 185 (2008).

[9] M. B. Chadwick, H. H. Barschall, R. S. Caswell *et al.*, Med. Phys. **26**, 974 (1999).

[10] Jingshang Zhang, Yinlu Han, and Ligang Cao, Nucl. Sci. Eng. **133**, 218 (1999).

[11] J. J. Griffin, Phys. Rev. Lett. **17**, 478 (1966).

[12] W. Hauser and H. Feshbach, Phys. Rev. **87**, 366 (1952).

[13] D. R. Tilley *et al.*, Nucl. Phys. **A708**, 3 (2002).

[14] D. R. Tilley *et al.*, Nucl. Phys. **A745**, 155 (2004).

[15] Zhang Jingshang and Han Yinlu, Commun. Theor. Phys. **36**, 437 (2001).
[16] Zhang Jingshang and Han Yinlu, Commun. Theor. Phys. **37**, 465 (2002).
[17] Zhang Jingshang, Commun. Theor. Phys. **39**, 433 (2003).
[18] Zhang Jingshang, Commun. Theor. Phys. **39**, 83 (2003).
[19] Sun Xiao-Jun, Duan Jun-Feng, Wang Ji-Min, and Zhang Jing-Shang, Commun. Theor. Phys. **48**, 534 (2007).
[20] Yan Yun-Liang, Duan Jun-Feng, Sun Xiao-Jun, Wang Ji-Min, and Zhang Jing-Shang, Commun. Theor. Phys. **44**, 128 (2005).
[21] Duan Jun-Feng, Yan Yun-Liang, Wang Ji-Min, Sun Xiao-Jun, and Zhang Jing-Shang, Commun. Theor. Phys. **44**, 701 (2005).
[22] Duan Junfeng, Yan Yuliang, Sun Xiaojun, Zhang Yue, and Zhang Jingshang, Commun. Theor. Phys. **47**, 102 (2007).
[23] Zhang Jing-Shang (private communication).
[24] Shen Qing-Biao, Nucl. Sci. Eng. **141**, 78 (2002).
[25] G. Audi, A. H. Wapstra, and C. Thibault, Nucl. Phys. **A729**, 337 (2003).
[26] ENDF-6 Formats Manual, Document ENDF-102, Report BNL-NCS-44945-05-Rev, 2005.
[27] J. S. Zhang and Y. Q. Wen, Chin. J. Nucl. Phys. **16**, 153 (1994).
[28] J. S. Zhang and S. J. Zhou, Chin. J. Nucl. Phys. **18**, 28 (1996).
[29] R. C. Haight, S. M. Grimes, R. G. Johnson *et al.*, Nucl. Sci. Eng. **87**, 41 (1984).
[30] M. C. Schell *et al.*, Med. Phys. **17**, 1 (1990).
[31] F. P. Brady *et al.*, Final report to the National Cancer Institute, Grant No. IR01 CA16261 (1979).
[32] I. Slypen, S. Benck, J. P. Meulders *et al.*, Phys. Med. Biol. **45**, 577 (2000).
[33] G. Börker, R. Böttger *et al.*, Radiat. Prot. Dosim. **23**, 23 (1988).
[34] Ali. S. Meigooni, J. S. Petler, and R. W. Finlay, Phys. Med. Biol. **29**, 643 (1984).
[35] J. J. Broeres *et al.*, *Nuclear Data for Neutron Therapy: Status and Future Needs.* IAEA-TECDOC-992 (IAEA, Vienna, 1997).
[36] J. S. Zhang and X. Z. Yang, Z. Phys. A **329**, 69 (1988).
[37] Z. Y. Sun, S. N. Wang, J. S. Zhang, and Y. Z. Zhuo, Z. Phys. A **305**, 61 (1982).
[38] J. S. Zhang, Sci. China Ser. G: Phys. Mech. Astron. **47**, 137 (2004).
[39] J. S. Zhang, J. M. Wang, and J. F. Duan, Commun. Theor. Phys. **48**, 33 (2007).
[40] A. Iwamoto and K. Harada, Phys. Rev. C **26**, 1821 (1982).
[41] Jingshang Zhang, Nucl. Sci. Eng. **142**, 207 (2002).